Pergamon

Chemical Engineering Science, Vol. 50, No. 17, pp. 2731–2746, 1995

0009–2509/95 $9.50 + 0.00

0009–2509(95)00041–0

HYDRODYNAMICS AND SELECTIVITY OF ANTIPOLARIZATION DIALYSIS

LUDWIG C. NITSCHE and SHAN ZHUGE
Department of Chemical Engineering, The University of Illinois at Chicago, 810 South Clinton Street, Chicago, IL 60607, U.S.A.

(*Received* 8 *February* 1994; *accepted* 21 *April* 1994)

Abstract—This paper represents a numerical investigation of the hydrodynamics and mass transfer operative in antipolarization dialysis ("APD"), a novel concept for fractionation in which adjacent countercurrent flow streams are (i) separated by a longitudinal solute-selective membrane, and (ii) pass through upstream and downstream "barrier" membranes that reject all solutes. Selectivity of the process—embodied in the sensitivity of steady-state concentration profiles to Péclet number and membrane transport resistance—has previously been analyzed (Nitsche, L. C., 1994, *Quart. Appl. Math.*, LII, 83–102) using the simplifying idealization of plug flow. Practical considerations of construction require the barrier membranes to be positioned longitudinally instead of transversely, so that the corresponding ultrafiltration flows occur perpendicular to the fully developed, parabolic velocity profiles in the channels. These hydrodynamic end effects are modeled numerically using a least-squares boundary singularity method that explicitly incorporates the analytical structure of discontinuities in the flow field arising at the junctions between porous and impermeable boundaries. Subsequently, the impact of flow nonidealities upon the transport of solute is addressed by applying finite differences to the relevant elliptic convection–diffusion equation for the concentration field. Calculations at large values of the aspect ratio take advantage of the singular asymptotic structure of the problem, whereby only the "inner" behavior at the ends of the flow channel is treated with a fine mesh in the longitudinal coordinate; a smoothly expanded mesh is sufficient for resolving the "outer" behavior in between. The grid is also selectively refined near the singularities in the convective coefficients. At unit Péclet number (based upon width of the flow channels) the resulting selectivity curves are found to be in remarkably close quantitative agreement with those for plug flow, despite major differences in the inner solute concentration profiles—a feature that does not persist at significantly higher Péclet numbers. Drawing an analogy with sedimentation–diffusion processes in rotating cylinders, the underlying mechanism of antipolarization is interpreted in terms of a circulation-flux parameter. In this way we illuminate the apparent robustness of the fractionation scheme with respect to details of the convective field.

INTRODUCTION

A recent paper (Nitsche, 1994a) has developed the theoretical basis of a new membrane-based fractionation concept which can be regarded as modifying countercurrent dialysis through the inclusion—in addition to the solute-selective membrane separating the opposite flow streams— of non-solute-selective membrane barriers at the ends of each flow channel. The latter allow only solvent to pass through the upstream and downstream ends, rejecting all of the dissolved species that are involved in the fractionation. In the absence of macrosolute diffusion from one side to the other, the flow fields would confine dissolved matter within thin layers at the two downstream barriers [Fig. 1(a)]. This represents the base flow that is modulated by diffusion across the longitudinal membrane: small lateral diffusional resistance of a particular solute means that the highly polarized condition of Fig. 1(a) cannot be sustained at steady state, and the resulting concentration profile must be much more uniform. The solute is then effectively levitated against the pull of the flow field, or "antipolarized" [Fig. 1(b)]—hence the term "antipolarization dialysis", or "APD".

The sensitivity of the concentration profiles to membrane transport resistance and Péclet number provides a means of fractionation that simultaneously exploits the selective modes of (i) dialysis and (ii) a simple version of SPLITT fractionation (Giddings, 1988)—while performing the function of solvent removal that is necessary for stagewise operation of the former (Noda and Gryte, 1981). For example, calculations based upon the simplifying assumption of plug flow (Nitsche, 1994a) indicate that for unit Péclet number based upon the *width* of the channel, good selectivity with respect to membrane transport resistance is obtained if the aspect ratio (streamwise/transverse dimension) is at least 10. Furthermore, the concentration profiles are very nearly uniform in the transverse direction, i.e. there is essentially no accumulation of rejected solute along the solute-selective membrane—except, of course, in the immediate vicinity of the downstream boundary layers. One should therefore expect the selectivity of APD to be largely unaffected by concentration polarization. In this connection it is relevant to mention a pertinent paper by Shaw *et al.* (1972), in which a different scheme for mitigating the effects of concentration polarization

was proposed and analyzed theoretically. Their approach involved the use of alternating sections of rejecting and nonrejecting membranes in series in order to draw off the accumulated concentration boundary layers. In both cases one sees the benefit of augmenting solute-selective membrane transport with an additional phenomenon—the latter being *relegated to a different membrane* in the same device. Other schemes, whereby the functions of solvent removal and solute removal are divided between different unit operations, have also been considered (Ray *et al.*, 1991).

As with conventional parallel-plate dialyzers (Klein *et al.*, 1987), a large-scale implementation of the APD separation concept would combine many narrow flow channels in parallel, interleaved between solute-selective membranes. Continuous operation would entail a carrier flow field perpendicular to the plane of Fig. 1, with splitting of the outlet stream into two or more fractions (Fig. 2). Thus we see that flow resistance of the barrier membranes does not place any direct limit on throughput. In classifying this implementation of APD we note that two basic elements are shared with the techniques of flow field-flow fractionation (Giddings *et al.*, 1976a, b, 1977a–c; Lee and Lightfoot, 1976; Wahlund *et al.*, 1986; Giddings, 1993) and SPLITT fractionation (Giddings, 1986): (i) selective flow-induced polarization of macrosolutes toward an ultrafiltration membrane, and (ii) outlet stream splitting into different fractions. The design and construction of flow cells would also be approached in a similar manner—to be discussed below. There is, however, a crucial distinction in the basic mechanism of ADP:

- The cross flows in FFF and SPLITT cause selective *transverse* polarization of solutes, and outlet stream splitting is carried out in the *short* dimension of the cross section.
- With APD the countercurrent flows cause *longitudinal* "piling-up"(modulated by transverse diffusion), and splitting occurs in the *long* dimension.

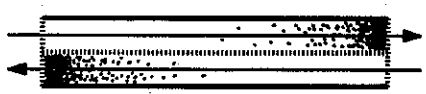

(a) Oppositely polarized

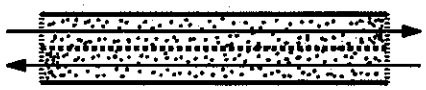

(b) Antipolarized

Fig. 1. Mechanism of antipolarization dialysis. In these two schematic drawings, the permeability of the longitudinal membrane to solute is (a) low vs (b) high.

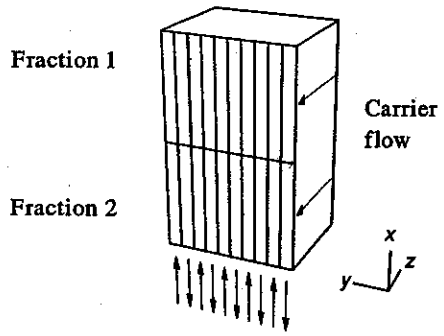

Fig. 2. Schematic illustration of APD adapted for continuous fractionation.

This feature of APD has advantages for the collection of multiple fractions.

In considering hydrodynamics and solute transport for comparison with the original plug-flow model (Nitsche, 1994a), we shall confine the present analysis to the steady-state concentration profile in the xy cross section in Fig. 2, in the absence of flow in the z direction and of any edge effects associated with finite depth in z. This problem embodies the essential mechanism of selectivity.

GEOMETRY OF A PROTOTYPICAL APD FLOW CELL

Considerations of design and construction of an APD flow cell are strongly influenced by the desire to have $O(1)$ Péclet number P based upon the width H^* of the channels (cf. Note 1 added in proof),

$$P = V^*H^*/D. \tag{1}$$

Given the small diffusivities D characteristic of macrosolutes, practical lower limits on the polarization-flow velocity V^* then place an upper bound on H^*. Realistic parameter values appear in Table 1. Channel widths on the order of fractions of a millimeter are routinely employed in FFF and SPLITT fractionation, formed by the void space between flat plates (solid or porous surfaces) that are clamped together and separated by one or more perforated spacers cut from thin sheets of metal or plastic. With this method of construction, however, it seems impractical to position the barrier membranes transversely (Fig. 1)—which represents the simplest model consistent with the idealization of plug flow (Nitsche, 1994a). Thus, we are led to consider a modification of the system, involving *longitudinal* barrier membranes, with the inflow and outflow of each channel occurring in the transverse direction (Fig. 3).

The purpose of this paper is to present a detailed numerical analysis of the hydrodynamics and resulting solute-transport behavior for the modified APD concept. In particular, we shall compare the selectivity with respect to membrane transport resistance with that for the "ideal" case of plug flow. Plug flow represents a useful assumption in conventional dialysis; see Hermans (1979). With reference to hollow-fiber units,

Table 1. Representative parameters for APD, computed for rigid spheres within the size range of proteins (e.g. bovine serum albumin), polysaccharides (e.g. dextran, ficoll), and asphaltenes; cf. Bohrer *et al.* (1984), Deen (1987) and King (1988)

Stokes–Einstein radius (Å)	Péclet number P	Membrane # 1 diffusional resistance $R^{[1]}$	Membrane # 2 transport resistance $R^{[2]}$
10	1.41	3.47×10^1	2.01
20	2.82	7.36×10^1	2.41
30	4.24	1.88×10^2	2.92
40	5.65	6.25×10^2	3.58
50	7.06	3.13×10^3	4.46
60	8.48	3.52×10^4	5.62
70	9.89	5.70×10^6	7.21
80	11.3	∞	9.40
90	12.7	∞	1.25×10^1
100	14.1	∞	1.69×10^1
110	15.5	∞	2.35×10^1
120	17.0	∞	3.35×10^1
130	18.4	∞	4.92×10^1
140	19.8	∞	7.46×10^1
150	21.2	∞	1.18×10^2

Note: Computations of Péclet number are based upon (i) channel width $H^* = 0.3$ mm; (ii) polarization flow velocity $V^* = 1$ μm/s; (iii) physical properties of water at room temperature. Giddings *et al.* (1976 a, b, 1977a–c), Lee and Lightfoot (1976) give analogous parameters for flow FFF. Membranes "#1" and "#2" refer to the relevant nominal parameters describing two specific Nuclepore® track-etched polycarbonate membranes (Costar, 1992): (i) pore diameter $d_p^{[1]} = 0.015$ μm, $d_p^{[2]} = 0.05$ μm; (ii) areal number density $n_p^{[1]} = n_p^{[2]} = 6 \times 10^{12}\,\mathrm{m}^{-2}$; (iii) thickness $\ell^{*[1]} = \ell^{*[2]} = 6$ μm.

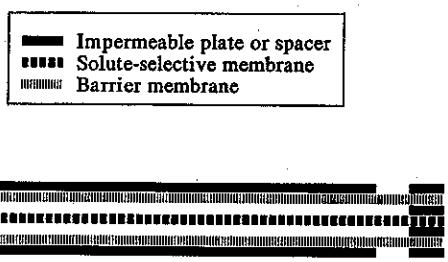

Fig. 3. Schematic illustration of plate-and-spacer construction of an APD cell. The upstream and downstream barrier membranes are positioned longitudinally rather than transversely (cf. Fig. 1), so that the flow in each channel must now undergo two right-angle bends.

previous theoretical and experimental investigations [see e.g. Noda *et al.* (1979) and Park and Chang, (1986)] have addressed other kinds of flow nonidealities on a much larger scale, regarding individual fibers essentially as constituting "microstructure" in a multiphase system. Nevertheless, the latter paper—which deals with flow in the distribution manifolds—has a significant element in common with our problem: the upstream and downstream surfaces of the fiber bundle are modeled as porous walls on the "macroscopic" scale.

HYDRODYNAMIC FORMULATION

We regard the fluid mechanics as providing the convective terms for the subsequent analysis of solute transport—tacitly assuming that the latter phenomenon does not significantly affect the former. As with the cross-flow based fractionation techniques mentioned above, the process of antipolarization dialysis is assumed to occur in the creeping-flow regime.

Position, velocity and pressure are made dimensionless using the channel width H^*, mean longitudinal velocity V^*, and viscous pressure scale $\mu V^*/H^*$, respectively. In these units the length $L = L^*/H^*$ of the channel also represents the aspect ratio. We pose the Stokes equations within the entrance region $0 < x < T$ (Fig. 4), matching the solution with the fully developed parabolic velocity profile (with unit

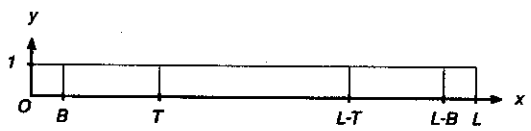

Fig. 4. Domain of solution, consisting of one of the two flow channels in Fig. 3. The entrance and exit regions are given by $0 < x < T$ and $L - T < x < L$, respectively. Flow occurs through the porous sections $0 < x < B$, $L - B < x < L$ of the upper wall. The flow fields at the ends are matched to a fully developed parabolic velocity profile in the middle section, along $x = T$ and $x = L - T$, for which $T = B + 3$ was found to be sufficiently large to encompass the entire flow rearrangement without introducing any significant inaccuracies in the matching.

total flux) at $x = T$; there is no slip at the impermeable wall $x = 0$.

$$\nabla^2 \mathbf{v} = \nabla p, \qquad \nabla \cdot \mathbf{v} = 0, \quad 0 < x < T, \; 0 < y < 1 \tag{2}$$

$$v_x(0, y) = 0, \qquad v_y(0, y) = 0, \quad 0 < y < 1 \tag{3}$$

$$v_x(T, y) = 6y(1 - y), \qquad v_y(T, y) = 0, \quad 0 < y < 1. \tag{4}$$

We assume that there is also no slip along the porous surfaces (Colton *et al.*, 1971; Lee and Lightfoot, 1976). The normal flux through each membrane can be assumed to be proportional to the local transmembrane pressure drop,

$$v_\perp^* = (K^*/\mu)\Delta p^*, \qquad v_\perp = K\Delta p \quad \text{with} \quad K = K^*/H^*. \tag{5}$$

Typical permeabilities of ultrafiltration membranes are sufficiently low that permeation through the solute-selective membrane ($y = 0$) can safely be neglected (Hermans, 1979; King, 1988; Costar, 1992). Furthermore, the pressure drop that is required to drive solvent through the barrier membrane ($y = 1$, $0 < x < B$) so vastly exceeds any pressure variations within the channel that the membrane behaves essentially like a perfect flow distributor, giving a uniform entrance velocity profile. Therefore, the set of boundary conditions is completed by stipulating that

$$v_x(x, 0) = 0, \quad v_y(x, 0) = 0, \qquad 0 < x < T \tag{6}$$

$$v_x(x, 1) = 0, \quad 0 < x < T,$$

$$v_y(x, 1) = \begin{cases} -B^{-1}, & 0 < x < B \\ 0, & B < x < T. \end{cases} \tag{7}$$

Fore-aft symmetry then gives the velocity field in the exit region, $L-T < x < L$.

Discontinuities and reformulation

Boundary conditions (3) and (7) embody discontinuities in the y velocity component at the two points $\mathbf{r}_1 = (0, 1)$ and $\mathbf{r}_2 = (B, 1)$. These discontinuities represent the macroscopic manifestation of the fine-scale flow field in the immediate vicinity of each transition between the permeable barrier membrane and an impermeable wall. Straightforward scaling arguments establish the basic asymptotic behavior,

$$\mathbf{v}(\mathbf{r}; K) \sim \tilde{\mathbf{v}}[K^{-1}(\mathbf{r} - \mathbf{r}_i)], \quad p(\mathbf{r}; K) \sim K^{-1}\tilde{p}[K^{-1}(\mathbf{r} - \mathbf{r}_i)]$$
$$\text{as } K \to 0; \quad \|\mathbf{r} - \mathbf{r}_i\| = O(K).$$

The $O(1)$ variation in velocity gives the macroscopic appearance of an angular discontinuity in velocity, whereby the (finite) limit as $\|\mathbf{r} - \mathbf{r}_i\| \to 0$ depends upon the direction of approach. Correspondingly, the $O(K^{-1})$ variation in pressure appears like an effectively infinite spike in the pressure for exceedingly small values of K. The analytical structure of this type of singularity is now well understood; it is usually associated with moving solid–fluid–solid contact lines (cf. Taylor, 1958, 1960; Moffat, 1964; Pan and Acrivos, 1967; Hancock *et al.*, 1981; Gupta *et al.*, 1981; Harper and Wake, 1983), and has the following general form:

Stream function

$$\Psi(x, y) = Ax + By + (Cx + Dy)\theta(x, y)$$

Velocity

$$V_x(x, y) = -B - D\theta(x, y) - (Dxy + Cx^2)/[r(x, y)]^2$$

$$V_y(x, y) = A + C\theta(x, y) - (Cxy + Dy^2)/[r(x, y)]^2$$

Pressure

$$P(x, y) = -2(Cx + Dy)/[r(x, y)]^2. \tag{8}$$

Table 2 gives the respective values of the constants A–D for the two discontinuities. On the $O(K)$ lengthscale there is a rapidly varying but finite "inner" solution for which the boundary condition (7) is modified by the seepage condition (5). This solution should be matched to the asymptotic behavior associated with the inner limit of the "outer" solution (8); see e.g. Bruns (1980) in connection with an analogous problem of piston-driven flow. The corner $\mathbf{r}_0 = (0, 0)$ is also a singular point, but there the magnitude of the inner solution (seepage flow across the solute-selective membrane) is determined by the *finite* inner limit of the outer pressure field—whereby the inner velocity field is asymptotically negligible, viz.

$$\mathbf{v}(\mathbf{r}; K) \sim K\tilde{\mathbf{v}}[K^{-1}(\mathbf{r} - \mathbf{r}_0)], \quad p(\mathbf{r}; K) \sim \tilde{p}[K^{-1}(\mathbf{r} - \mathbf{r}_0)]$$
$$\text{as } K \to 0; \; \|\mathbf{r} - \mathbf{r}_0\| = O(K).$$

These fine-scale details are avoided here: exploiting linearity, we simply regularize the (outer) hydrodynamic problem by writing the unknown solution as the sum of

(i) a base flow field ("B") obtained by superposing the two angular singularities from eq. (8) and Table 2 as well as a uniform flow in the $+y$ direction and the fully developed parabolic velocity profile (4);

Table 2. Constants for the two kinds of singularities in the entrance flow field that arise at the junctions between solid vs permeable sections of the left and top boundaries; see eq. (8)

Type i	Location (x, y)	A_i	B_i	C_i	D_i
1	(0, 1)	-1	$(\pi/2)/(\pi^2/4 - 1)$	$-(\pi/2)/(\pi^2/4 - 1)$	$1/(\pi^2/4 - 1)$
2	(B, 1)	0	$-1/\pi$	$1/\pi$	0

(ii) the remaining disturbance field which is now continuous along the boundary.

Explicitly, we have

$$\psi(x, y) = \psi^{(B)}(x, y) + \phi(x, y)$$
$$\mathbf{v}(x, y) = \mathbf{v}^{(B)}(x, y) + \mathbf{u}(x, y) \tag{9}$$

where

$$\psi^{(B)}(x, y) = [\Psi(x, y-1; \mathscr{C}_1) + \Psi(x-B, y-1; \mathscr{C}_2) + x]B^{-1} + y^2(2y-3)$$
$$\mathbf{v}^{(B)}(x, y) = [\mathbf{V}(x, y-1; \mathscr{C}_1) + \mathbf{V}(x-B, y-1; \mathscr{C}_2) + \mathbf{e}_y]B^{-1} + 6y(1-y)\mathbf{e}_x \tag{10}$$

with $\mathscr{C}_k$ representing the set of four constants $\{A_k, B_k, C_k, D_k\}$. Figure 5 shows streamlines for $\mathbf{v}^{(B)}(x, y)$, whose boundary values must now also be cancelled out in writing boundary conditions analogous to eqs (3), (4), (6), (7) for $\mathbf{u}(x, y)$. The new hydrodynamic problem has continuous boundary data. In connection with this general approach to the incorporation of singular behavior into numerical solutions of hydrodynamic problems, see e.g. Bruns (1979) and Ingham and Kelmanson (1984, Chap. 3).

Least-squares boundary singularity method

The method of fundamental solutions as applied to Stokes flow is reviewed in the recent monograph of Pozrikidis (1992, Chap. 7); details on the least-squares variant in specific applications appear in a number of papers, including Dąbroś (1985) and Nitsche and Brenner (1990). Thus, the following discussion is confined to the most salient features of the problem at hand.

Exploiting the linearity of the Stokes equations, the approximate solution in the domain is expressed as the superposition of singular solutions whose poles are distributed along a curve that lies *behind* the physical boundary on which the boundary conditions are imposed. Corresponding to each pole $\hat{\mathbf{r}} = (\hat{x}, \hat{y})$ we have three basis solutions: [1] point source, [2] point force in the x direction, [3] point force in the y direction. Their respective stream functions, velocity components and pressure fields are given by the formulas (see e.g., Pozrikidis, 1992, pp. 60, 61, 199)

$$\Psi^{[1]}(\mathbf{R}) = -\theta(X, Y), \qquad \Psi^{[2]}(\mathbf{R}) = Y(\ln R - 1),$$
$$\Psi^{[3]}(\mathbf{R}) = -X(\ln R - 1), \qquad U_x^{[1]}(\mathbf{R}) = XR^{-2},$$
$$U_x^{[2]}(\mathbf{R}) = X^2R^{-2} - \ln R, \qquad U_x^{[3]}(\mathbf{R}) = XYR^{-2},$$
$$U_y^{[1]}(\mathbf{R}) = YR^{-2}, \qquad U_y^{[2]}(\mathbf{R}) = XYR^{-2}, \tag{11}$$
$$U_y^{[3]}(\mathbf{R}) = Y^2R^{-2} - \ln R, \qquad P^{[1]}(\mathbf{R}) = 0,$$
$$P^{[2]}(\mathbf{R}) = 2XR^{-2}, \qquad P^{[3]}(\mathbf{R}) = 2YR^{-2}$$

with $\mathbf{R} = (X, Y) = (x - \hat{x}, y - \hat{y})$ and $R = \sqrt{X^2 + Y^2}$. For each pole care is taken that the branch cut of the polar angle function $\theta(x - \hat{x}, y - \hat{y})$ points away from the fluid domain.

The distributions of poles $\{\hat{\mathbf{r}}_1, \ldots, \hat{\mathbf{r}}_J\}$ are shown in Fig. 5 for two particular sets of parameters. The (regularized) solution $\mathbf{u}(\mathbf{r})$, eq. (9) is expressed as a linear combination of the singular basis functions $\mathbf{U}^{[i]}(\mathbf{R}_j) = \mathbf{U}^{[i]}(\mathbf{r} - \hat{\mathbf{r}}_j)$ centered at the poles $\hat{\mathbf{r}}_1, \ldots, \hat{\mathbf{r}}_J$, viz.

$$\mathbf{u}(\mathbf{r}) = \sum_{i=1}^{3} \sum_{j=1}^{J} A_{i,j}\mathbf{U}^{[i]}(\mathbf{r} - \hat{\mathbf{r}}_j). \tag{12}$$

An analogous superposition formula applies to the stream function $\phi(x, y)$.

The coefficients $A_{i,j}$ are optimized in a least-squares sense with respect to an excess of boundary criteria corresponding to the analogs of eqs (3), (4), (6), (7) for $\mathbf{u}(\mathbf{r})$ imposed at discrete points. This is done by applying a LINPACK QR algorithm (Dongarra *et al.*, 1979, Chap. 9) to the rectangular matrix whose rows and columns are associated with the individual boundary criteria and unknown coefficients, respectively. In the calculations reported here, the number of rows exceeded the number of columns by more than

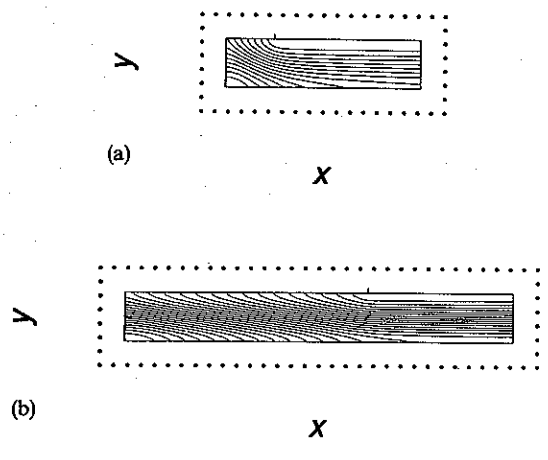

Fig. 5. Streamlines for the base flow field $\mathbf{v}^{(B)}(x, y)$ from eq. (10), and distribution of singularities: (a) $B = 1$, $T = 4$; (b) $B = 5$, $T = 8$.

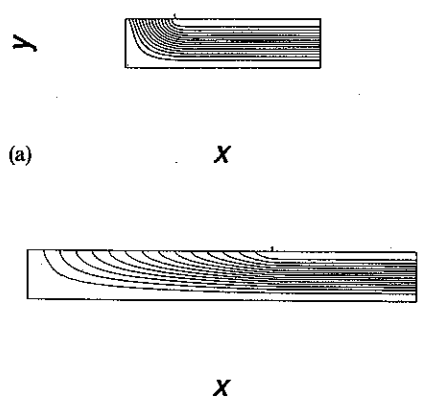

Fig. 6. Streamlines for the entrance flow field $\mathbf{v}(x, y)$ from eqs (9), (10) and (12): (a) $B = 1$, $T = 4$; (b) $B = 5$, $T = 8$.

a factor of 9, thereby affording greater robustness with respect to the positions of the boundary points than would simple collocation. Streamlines for the flow in the entrance region are shown in Fig. 6.

CONVECTION–DIFFUSION PROBLEM FOR SOLUTE TRANSPORT

Under the assumption of dilute solutions, the steady-state transport behavior of a particular solute is governed by a standard convection–diffusion equation (Bird *et al.*, 1960, Chap. 18),

$$\frac{\partial^2 c}{\partial x^2} + \frac{\partial^2 c}{\partial y^2} - Pv_x(x,y)\frac{\partial c}{\partial x} - Pv_y(x,y)\frac{\partial c}{\partial y} = 0, \quad 0 < x < L, \quad 0 < y < 1 \tag{13}$$

where central symmetry of the flow-cell geometry indicates the following relations for the flow and concentration fields on the other side ($y < 0$) of the solute-selective membrane:

$$\begin{aligned} v_x(x,y) &= -v_x(L-x, -y), \\ v_y(x,y) &= -v_y(L-x, -y), \\ c(x,y) &= c(L-x, -y). \end{aligned} \tag{14}$$

The concentration of solute is determined only within an arbitrary factor (mean concentration C^*) that sets the total amount in the flow cell; upon this basis the dimensionless concentration c is normalized according to

$$\frac{1}{L}\int_0^L \int_0^1 c(x,y)\,dx\,dy = 1. \tag{15}$$

For $O(1)$ spatial variations in $c(x,y)$, the flux of solute is referred to the diffusive scale C^*D/H^*. The Péclet number P is given by eq. (1); all other variables are nondimensionalized as before.

Because there is no flux of solute through the solid walls or barrier membranes, we have the following boundary conditions in consequence of eqs (3), (7):

$$\frac{\partial c}{\partial x}(0,y) = 0, \qquad \frac{\partial c}{\partial x}(L,y) = 0, \quad 0 < y < 1 \tag{16}$$

$$\frac{\partial c}{\partial y}(x,1) = \begin{cases} -Pc(x,1)/B, & 0 < x < B \\ 0, & B < x < L-B \\ Pc(x,1)/B, & L-B < x < L. \end{cases} \tag{17}$$

The latter condition, together with the discontinuous flow structures of the form (8), leads to finite jumps in the normal derivative and attendant weak singularities in the concentration field. Finally, in the absence of bulk seepage we have purely diffusive transport through the solute-selective membrane—driven by the local transmembrane Δc driving force. Utilizing central symmetry, eq. (14), we have

$$\frac{\partial c}{\partial y}(x,0) = \frac{1}{R}[c(x,0) - c(L-x,0)]. \tag{18}$$

The dimensionless diffusional resistance of the membrane is given by

$$R = \ell^*/(H^*\gamma\mathscr{H}), \tag{19}$$

with ℓ^* and γ the thickness and areal porosity of the membrane, respectively. The hydrodynamic hindrance factor $\mathscr{H}$ enters for solute particles that are of appreciable size compared with the characteristic pore diameter. Its estimation under various physical assumptions is discussed in the review article by Deen (1987)—including a simplified formula for spherical particles [Deen, 1987, eq. (2) in Table 1] that accounts only for centerline hydrodynamics but is nevertheless in good agreement with experimental data and more comprehensive theory. This equation has been used to calculate the representative values listed in Table 1.

NUMERICAL SOLUTION BY FINITE DIFFERENCES

The elliptic boundary-value problem formulated above is treated numerically here by finite differences. As the discretization is fairly standard [see e.g. Dahlquist and Björck (1974), Chaps 7, 8] the brief discussion here will focus on two issues that bear most specifically on the problem at hand: (i) scheme of mesh grading; and (ii) reformulation of the discretized equations in terms of an eigenvalue problem.

Grid generation and the discretized equations

Local expansion and compression of the grid (relative to the "base" spacing) is carried out as follows:

- The solution varies strongly only in the vicinity of the barrier-membrane ultrafiltration flows, taken to comprise the subregions $0 < x < 3B/2$ and $L - 3B/2 < x < L$. In between the mesh spacing is smoothly increased approaching the middle ($x = L/2$), at which the terminal mesh expansion factor is α. Formally, the boundary-value problem could be approached in a singular-perturbative manner—by matching "inner" solutions at the ends with an "outer" solution written using a stretched x coordinate in the middle. The expanded grid takes advantage of this feature to keep computer memory requirements within tractable limits.
- The mesh is refined in both the x and y directions (terminal compression factor β) in the vicinity of the flow-field singularities $(x,y) = (0,1)$, $(B,1)$, $(L-B,1)$, $(L,1)$, in order to better represent the associated weak singularities in the solute concentration field. Otherwise there seems to be numerical "leakage" of solute through the rejecting membranes.

For both variables the graded mesh is generated with an appropriate "stretching function" (Thompson *et al.*, 1985, Chaps V, VIII), whereby an evenly spaced mesh in transformed variables (ξ, η) leads to the desired nonuniform mesh in the physical-space coordinates (x, y).

$$\begin{aligned} x_i &= LF(\xi_i;\alpha,\beta), \quad \xi_i = i/m \ (i = 0,1,2,\ldots,m) \\ y_j &= G(\eta_j;\beta), \quad \eta_j = j/n \ (j = 0,1,2,\ldots,n). \end{aligned} \tag{20}$$

Correspondingly, the numbers of grid intervals m and n must be modified from the base values that correspond to a uniform square mesh,

$$m = \{M(\alpha, \beta)n_0 L\} \rightarrow \text{next higher even integer (if not even)}; \quad (21)$$
$$n = \{N(\beta)n_0\}$$

where the brackets $\{...\}$ denote the operation of rounding to the nearest integer. The composite stretching functions $F(\xi; \alpha, \beta)$ and $G(\eta, \beta)$ were generated by splicing together elementary transition functions of the type described in a recent paper (Nitsche, 1994b). The most salient features of this grid generation procedure are (i) advantageous placement of nodes considered with respect to either of two possible conceptions of truncation order [fixed relative distribution vs fixed number of nodes; see Thompson and Mastin (1985)]; and (ii) prescribed regularity at the matching points. Trials were made with C^2 and C^6 stretching functions, generated for both classes of truncation-error criteria. The C^2 grids based upon the fixed-number criterion were found to be the most robust. Mesh parameters are listed in Table 3, for which the associated grids appear in Fig. 7. The local density of grid points—determined by the slope of the relevant stretching function—refers to infinitesimal

Table 3. Mesh parameters

Mesh	Regularity	L	B	n_0	α	β	m	n
(a)	C^2	10	1	16	1.0	1.0	160	16
(b)	C^2	10	1	16	1.0	15.0	302	40
(c)	C^2	10	1	16	5.0	15.0	242	40
(d)	C^2	10	1	40	2.4	1.0	302	40
(e)	C^2	10	2/3	60	8.0	1.0	292	60
(f)	C^2	10	1	16	5.0	26.0	304	50
(g)	C^2	20	1	16	10.0	15.0	278	40
(h)	C^2	40	1	16	20.0	15.0	326	40
(i)	C^6	40	1	16	20.0	15.0	228	31

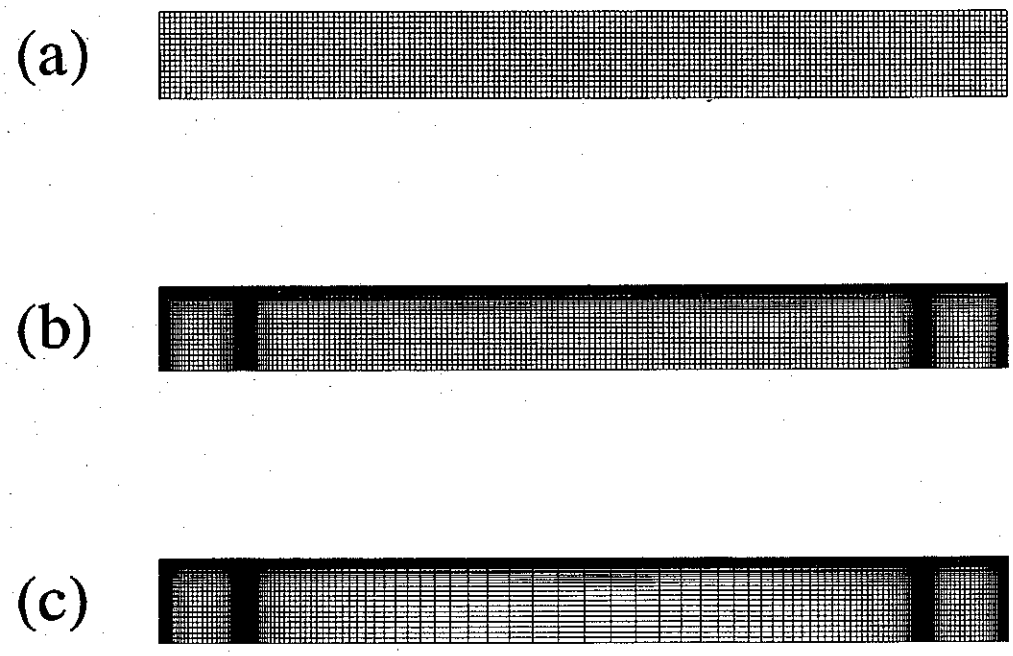

Fig. 7. Finite-difference grids corresponding to the parameter values listed in Table 3. For aspect ratios $L = 20, 40$ [grids (g)–(i)], the section shown ($0 \leqslant x \leqslant 10$) represents only part of the domain.

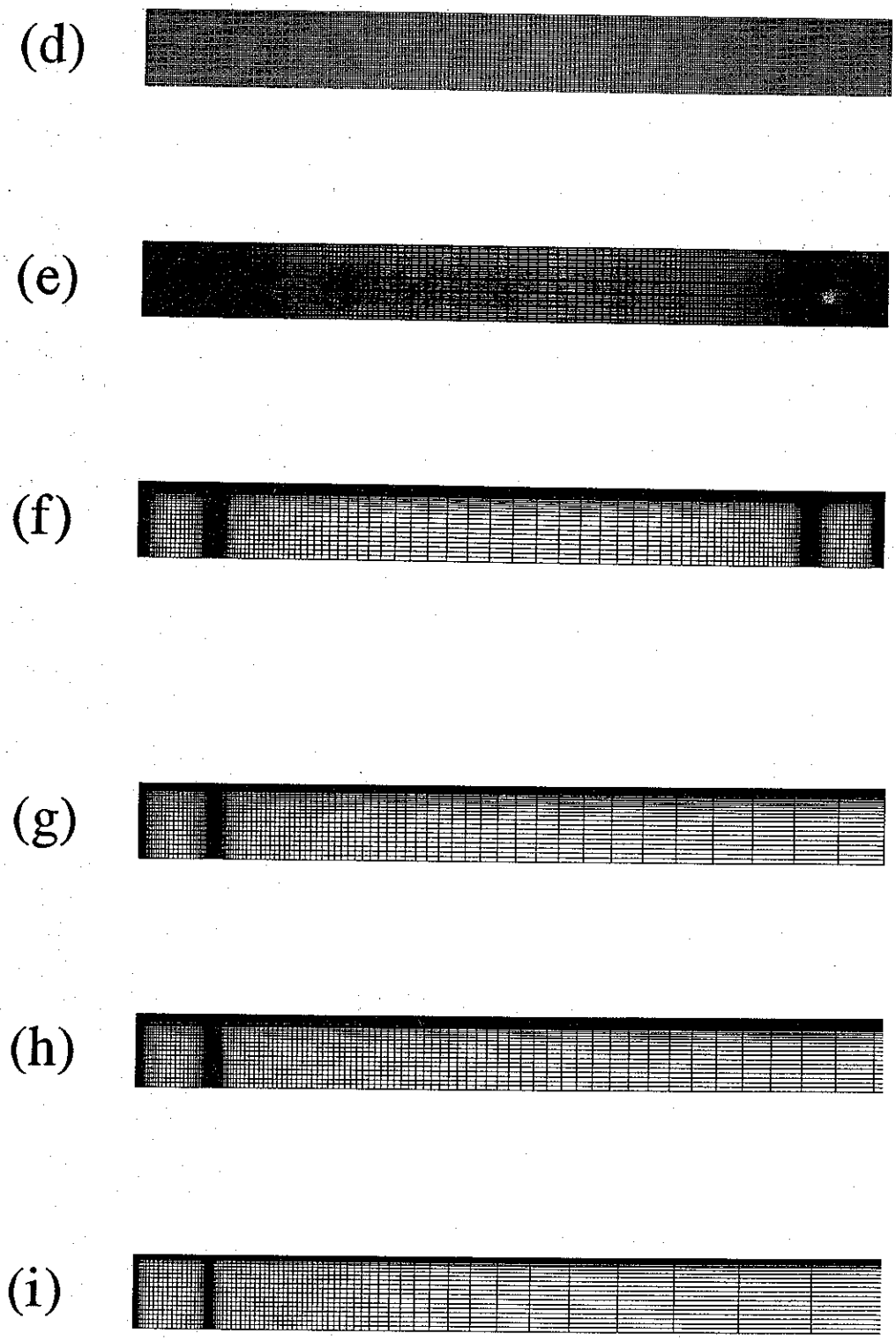

Fig. 7(d)–(i).

spacing: for any finite number of points the expansion and compression factors α and β are therefore only approximate.

The transformed, (ξ, η) version of the boundary-value problem involves metrical coefficients that contain derivatives of the stretching functions $F(\xi; \alpha, \beta)$ and $G(\eta; \beta)$. Considerations of truncation errors (Thompson *et al.*, 1985, Chap. V) indicate that these derivatives should *not* be evaluated analytically; rather, the finite-difference formulas used to discretize the differential equation and boundary conditions should be applied to the metrical coefficients as well. Although written for the (ξ, η) problem, the resulting difference approximations then do not explicitly involve the ξ_i or η_j from eq. (20). This is illustrated by the second-order central-difference formulas

$$\left[\frac{\partial c}{\partial x}\right]_{i,j} \approx \left[\frac{1}{x_{i+1} - x_{i-1}}\right] c_{i+1,j} - \left[\frac{1}{x_{i+1} - x_{i-1}}\right] c_{i-1,j}$$

$$\left[\frac{\partial^2 c}{\partial x^2}\right]_{i,j} \approx \left[\frac{8(x_{i+1} - x_i)}{(x_{i+1} - x_{i-1})^3}\right] c_{i-1,j} - \left[\frac{8}{(x_{i+1} - x_{i-1})^2}\right] c_{i,j} + \left[\frac{8(x_i - x_{i-1})}{(x_{i+1} - x_{i-1})^3}\right] c_{i+1,j}.$$

Boundary condition (18) requires no interpolation between node points owing to reflective symmetry of the mesh about $x = L/2$:

$$x_{m-i} = L - x_i.$$

The above discretization scheme corresponds to a "nonconservative" numerical formulation (Thompson *et al.*, 1985, Chaps III, IV). Finally, we mention that the boundary conditions were discretized at second order by two alternative schemes: (i) fictitious node points lying outside the domain to preserve the centered computational "molecule" of the differential equation (Dahlquist and Björck, 1974, pp. 320, 386) vs (ii) one-sided differences (Thompson *et al.*, 1985, pp. 142, 143). The two methods were checked for consistency of the results in a few test cases, but the former was used to generate the final results, because for a given mesh it resulted in a smaller bandwidth, by a factor of two, of the finite-difference coefficient matrix.

Eigenproblem reformulation of the discretized equations

The elliptic boundary-value problem (13), (16)–(18) could be rewritten more generally in terms of a differential/boundary operator,

$$\mathcal{L}[c] = 0.$$

Thus, the solution $c(x, y)$ that we seek resides in the nullspace of $\mathcal{L}$—the arbitrary multiplicative constant being determined by the normalization condition (15). It turns out that the finite-difference discretization of this equation yields a *nonsingular* coefficient matrix A. Ostensibly, the discrete version of condition (15) is then redundant, and upon discarding it we should find only the trivial solution for the homogeneous linear system. Indeed, it can readily be verified that the same feature is observed for the simplest analogous problem in one dimension with constant coefficients,

$$c''(x) - Pc'(x) = 0 \quad (0 < x < L);$$

$$c'(x) - Pc(x) = 0 \quad (x = 0, L).$$

By contrast, the case of pure diffusion ($P = 0$) leads to a singular finite-difference matrix, from which one linearly dependent row can be discarded to impose normalization.

Rather than (i) simply replacing one of the finite difference equations (i^*, j^*) with $c_{i^*,j^*} = 1$ (subject to *a posteriori* normalization), or (ii) applying all node equations plus normalization in a least-squares sense, a better approach is to approximate the discrete numerical solution by the eigenvector corresponding to the smallest eigenvalue of the coefficient matrix A. (This scheme was suggested to the authors by Professors Charles Tier and Floyd B. Hanson, Department of Mathematics, Statistics, and Computer Science, University of Illinois at Chicago.) As the mesh is made finer (with fixed relative distribution), $\lambda_{\min} \to 0$, and the corresponding eigenspace (of increasing dimension) becomes a better and better representation of the desired nullspace of the differential operator. A numerical test seemed to indicate the approximate scaling $\lambda_{\min} \propto n_0^{-4}$ over part of the range of n_0 investigated. Note that the discretized equations themselves are satisfied only to order $O(\lambda_{\min})$.

The smallest eigenvalue and corresponding eigenvector of the finite-difference matrix were obtained by inverse iteration (Jennings and McKeown, 1992, Chap. 9), using LINPACK bandsolving routines (Dongarra *et al.*, 1979, Chap. 2) to carry out the initial LU factorization and subsequent back substitutions. In the calculations pertaining to Figs 8, 10–13, below, the largest value of $\lambda_{\min}$ encountered was 7.5×10^{-7}. With no more than 9 iterations, an *a posteriori*, row-by-row check on the matrix eigenproblem indicated a relative error of less than 4×10^{-7} in all cases.

NUMERICAL RESULTS

Concentration profiles

Concentration profiles corresponding to the ("nonideal") flow field from Fig. 6(a) are depicted in Fig. 8. At both ends the lateral concentration gradients exactly balance convection in their respective ultrafiltration flows, eq. (17), while driving a purely diffusive flux (in, upstream vs out, downstream) through the solute-selective membrane, eq. (18). With reference to the schematic diagrams in Fig. 1, there is thus a net circulation of solute in the clockwise direction, which will be considered quantitatively in more detail, below.

The weak singularities associated with discontinuities in the normal derivative, eq. (17), appear like

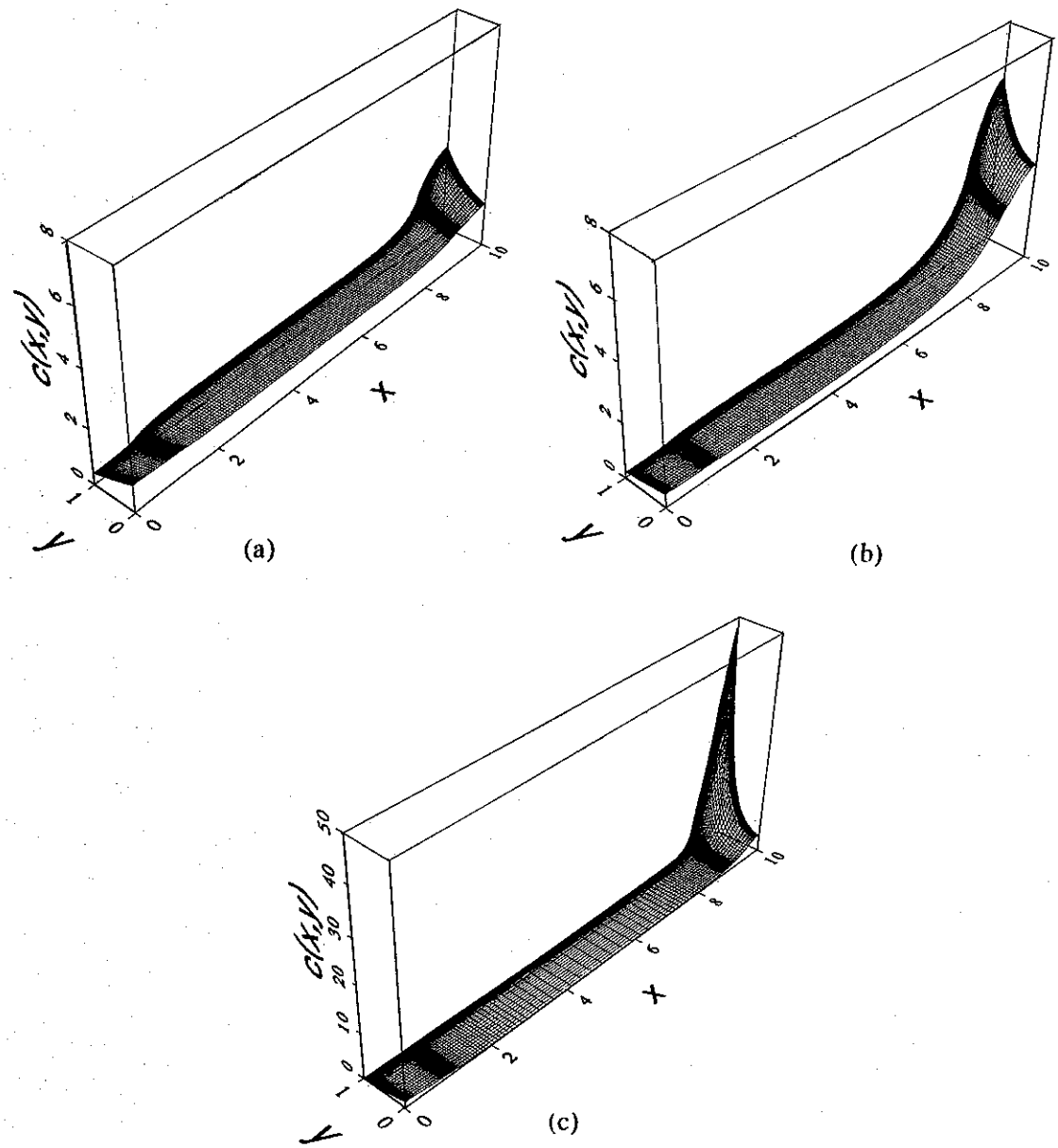

Fig. 8. Dependence of the concentration profile $c(x, y)$ upon Péclet number P and membrane diffusional resistance R at aspect ratio $L = 10$, for the "nonideal" flow field from Fig. 6(a): (a) $P = 1, R = 1$; (b) $P = 1, R = 10$; (c) $P = 5, R = 1$.

small wrinkles in the surface $c(x, y)$ at $(x, y) = (B, 1)$, $(L - B, 1)$. The other two singularities at $(x, y) = (0, 1), (L, 1)$ are not readily discernible, perhaps because they occur in corners of the domain.

At the same value of R, concentration polarization at the downstream barrier membrane is seen to be much stronger for $P = 5$ than for $P = 1$ [Figs 8(a),(c)]. The lateral polarization in Fig. 8 is to be contrasted with the longitudinal polarization that occurs for the simple idealization of plug flow, Fig. 9. Despite this major difference, however, at each value of R for $P = 1$ the respective solute concentration fields for ideal vs nonideal flow level off to very similar, nearly uniform levels as one moves away from the ends.

Testing of accuracy

For plug flow the finite-difference scheme was tested against the matched-eigenfunction-expansion solution of Nitsche (1994a) carried to 320 terms based upon a 390×390 linear system. Using grids (a) and (c) from Table 3 [Figs 7(a),(c)] comparisons with the series solution were carried out for $R = 1$ vs 10 at $P = 1$; the maximum absolute and percentage discrepancies in concentration encountered at any node point were less than 0.02 and 0.5%, respectively. This

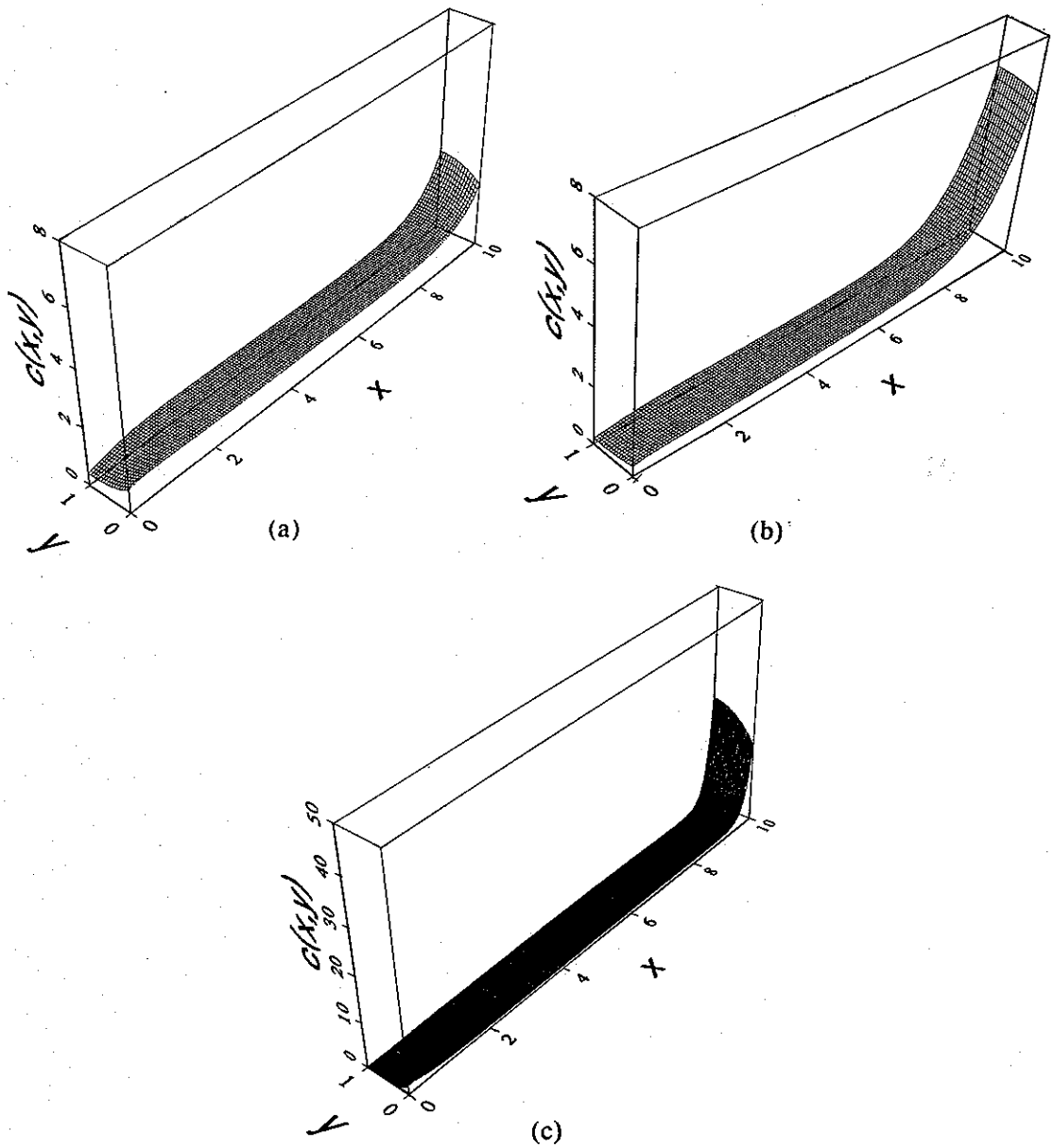

Fig. 9. Dependence of the concentration profile $c(x, y)$ upon Péclet number P and membrane diffusional resistance R at aspect ratio $L = 10$, for the idealized case of plug flow. (a) $P = 1, R = 1$; (b) $P = 1, R = 10$; (c) $P = 5, R = 1$.

procedure demonstrated the accuracy and mesh-independence of the numerical concentration profiles. Note that the local refinement zones in grid (c) are motivated by features of the *nonideal* flow field, Fig. 6(a), which have no counterpart for the transport problem with plug flow. (Large exponential factors and attendant round-off errors make the eigenfunction expansion scheme computationally intractable for PL substantially larger than 20.)

Overall mass conservation was also checked, embodied in the equality of longitudinal flux $J_\parallel$ and lateral flux $J_\perp$,

$$J_\parallel = \int_0^1 \left[PV_x(L/2, y)c(L/2, y) - \frac{\partial c}{\partial x}(L/2, y) \right] dy,$$
$$J_\perp = \int_{L/2}^{L} [c(x,0) - c(L-x,0)]\,dx \tag{22}$$

both of which represent the net clockwise circulation of solute referred to above. In none of the above four test cases was the difference between $J_\parallel$ and $J_\perp$ greater than 0.5%. This would seem to provide a particularly

stringent test at the larger value of R, for which stronger polarization means that no flux through the downstream barrier membrane represents the cancelling out of larger convective and diffusive counterfluxes. Furthermore, the percentage error is based upon the smaller circulation J. The accuracy of mass conservation deteriorated for Péclet number significantly greater than unity. Compared with grids (a) and (c) used for $P = 1$, the much more extensive grid (e) gave the discrepancy $\Delta J/J_{\|} = 1.6\%$ at $P = 5$ and $R = 1$; see Fig. 9(c).

The hydrodynamic end effects for nonideal flow make the solute transport problem more difficult. Of particular importance is the apparent numerical "leaking" of solute at the junctions between the barrier membranes and the solid walls—i.e. at the angular discontinuities in the convective coefficients. Strong polarization at the downstream end, observed for large values of the product PL, exacerbates the problem, for which localized mesh refinement near the singularities is effective. For example, for the case $L = 10$, $P = 5$, $R = 1$, grid (d), which is evenly spaced at the ends, gives a discrepancy $\Delta J/J_{\|} = 10.2\%$. For exactly the same number of nodes in x and y, the locally refined grid (b) gives $\Delta J/J_{\|} = 1.0\%$. With more nodes grid (f) yields $\Delta J/J_{\|} = 0.6\%$. Larger aspect ratios with $P = 5$ were problematic, so calculations for $L = 20$ and $L = 40$ are restricted to the case $P = 1$, for which (cf. Note 1 added in proof) behavior at $L = 10$ represents a useful indication of what could be expected at larger aspect ratios. In summary, the numerical results for nonideal flow were spot checked for mesh independence as follows: (i) grids (b) and (c) for $L = 10$, $P = 1$; (ii) grids (f) and (b) for $L = 10$, $P = 5$; (iii) grids (h) and (i) for $L = 40$, $P = 1$. The results presented in Figs 8, 10–13 were obtained using the former grid in each of these three cases, and using grid (g) for $L = 20$, $P = 1$. In all of these calculations $\Delta J/J_{\|}$ was less than 0.7%.

In order to assess the insensitivity of the finite-difference numerics to the method of discretization at the boundaries (discussed earlier), the lateral derivative along the solute-selective membrane, $(\partial c/\partial y)(x, 0)$, was evaluated by applying the *three-point, one-sided* difference formula to the numerical solution *obtained using the central-difference scheme and fictitious node points*. At each node along $y = 0$ this one-sided derivative was compared with the lateral flux required by the local transmembrane Δc driving force, eq. (18). The latter is an odd function of x about $x = L/2$, the maximum magnitude of which was used to normalize the biggest discrepancy in $(\partial c/\partial y)(x, 0)$ for a given concentration profile. This test was carried out for all of the calculations pertaining to Figs 8, 10–13, for which the normalized discrepancy did not exceed 6%. Integrated numerically using the *one-sided* derivatives, the upstream $(0 \leqslant x \leqslant L/2)$ and downstream $(L/2 \leqslant x \leqslant L)$ lateral fluxes—both supposing to represent the net circulation J— did not differ by more than 7% in any case. This check of consistency broke down at higher values of the membrane diffusional resistance R, which limited the range of results presented here.

Selectivity

A simple version of the stream-splitting scheme described in the Introduction (Fig. 2) would involve the collection of two equal fractions—upstream vs downstream—from each flow channel. The ratio of the respective amounts of a particular solute in the two samples, given by the average concentrations

$$\bar{c}_1 = \frac{2}{L}\int_0^{L/2}\int_0^1 c(x, y)\,dy\,dx,$$
$$\bar{c}_2 = \frac{2}{L}\int_{L/2}^{L}\int_0^1 c(x, y)\,dy\,dx = 2 - \bar{c}_1 \tag{23}$$

represents the separation factor for that species. Note that $\bar{c}_1$ can also be regarded as a dimensionless "degree of antipolarization", because a perfectly uniform (antipolarized) concentration profile would give $\bar{c} = 1$, whereas accumulation of all of the solute at the downstream barrier membrane would imply $\bar{c}_1 = 0$.

Selectivity of APD with respect to membrane permeability to solutes is given by the steepness of the graph of $\bar{c}_1$ vs the reduced diffusional resistance $R' = R/L$. This functional relationship plays a role analogous to the fractional extraction curve in conventional countercurrent dialysis (see Noda and Gryte, 1981; Nitsche, 1994a),

$$E = (1 + R'')^{-1}. \tag{24}$$

For aspect ratio $L = 10$, Fig. 10 shows the selectivity curves $\bar{c}_1(R')$ for $P = 1$ vs $P = 5$. The original concept of APD was based upon the assumption that $P \approx 1$, whereby the polarization layers are roughly as thick as the channel width H^*. This placed upper limits on the realistic values of H^* and the flow velocity V^*, as discussed above in connection with eq. (1). Clearly,

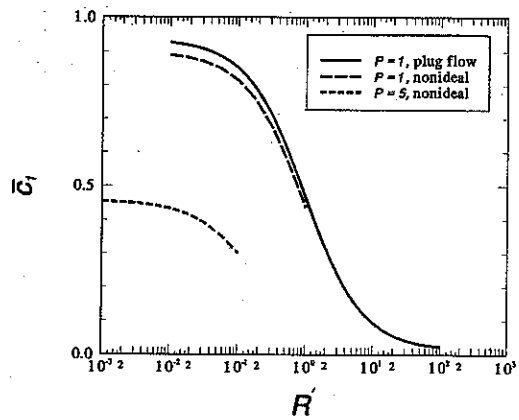

Fig. 10. Degree of antipolarization $\bar{c}_1$ as a function of reduced diffusional resistance R' at two values of the Péclet number, $P = 1$ vs 5, for the "nonideal" flow field from Fig. 6(a). For comparison, the curve for $P = 1$ in the idealized case of plug flow is also shown. In all cases $L = 10$. Selectivity is determined by the steepness of the curves.

good selectivity at higher Péclet number would significantly broaden the physically useful parameter space. In this connection we note that the steepness of the curve for $P = 5$ is roughly half that for $P = 1$; with staging this reduction in separation efficiency could easily be overcome. (Horizontal shifts between the curves do not impact on the selectivity with respect to R' at fixed P.) Comparing the selectivity curves for ideal vs nonideal flow for $L = 10$ and $P = 1$, one sees that the major differences between the polarization behavior at the ends, Figs 8(a),(b) vs 9(a),(b), do not impact strongly on the gross features of the concentration profiles that determine selectivity. Evidently, at unit Péclet number the primary aspect of APD is the modulation by lateral diffusion of solute accumulation at the downstream ends of the narrow flow channels; precise details of positioning the barrier membranes are only of secondary importance. Thus, the basic mechanism is seen to be quite robust with respect to details of implementing the desired flow field. This feature does not persist to higher Péclet numbers: for the same membrane resistance $R = 1$, the concentration profiles in Fig. 8(c) vs 9(c) correspond to $\bar{c}_1 = 0.30$ vs 0.54, respectively.

The effect of aspect ratio L upon the selectivity curves, with fixed Péclet number $P = 1$, is shown in Fig. 11. The curves become steeper, approaching the fractional extraction curve for conventional dialysis as L is made larger. It is reasonable to suppose that sufficiently large aspect ratios (easily achievable in practice) should yield selectivity with respect to membrane diffusional resistance R at fixed P that is essentially indistinguishable from that for dialysis.

The selectivity of APD with respect to Péclet number at fixed membrane diffusional resistance ($R = 1$) is shown in Fig. 12 for the aspect ratio $L = 10$. It is illuminating to compare the curve of $\bar{c}_1$ vs P with analogs in the relevant version of SPLITT fractionation (Giddings, 1985, 1988). In the present context the SPLITT approach can be regarded as involving only the polarization equilibrium (without selective membrane diffusion) to achieve differential segregation of a particular solute between two fractions. As observed in the Introduction, the polarization and sample splitting occur in the *transverse* direction, as opposed to the schematic drawing of APD in Fig. 2. In what then corresponds to an "equilibrium mode" of operation of SPLITT (Giddings, 1988), described by the Boltzmann-type lateral concentration profile,

$$c(y) = \frac{P}{e^P - 1} e^{Py}$$

the segregation of solute is determined by the respective average concentrations

$$\bar{c}_1' = \frac{1}{1-\Omega}\int_0^{1-\Omega} c(y)\,dy = \frac{1}{1-\Omega}\frac{e^{P(1-\Omega)} - 1}{e^P - 1},$$

$$\bar{c}_2' = \frac{1}{\Omega}\int_{1-\Omega}^{1} c(y)\,dy = \frac{1 - (1-\Omega)\bar{c}_1'}{\Omega}.$$

Here Ω represents the fractional thickness of the latter zone (containing the polarization layer). Curves of $\bar{c}_1'$ vs P are shown in Fig. 12 for $\Omega = 0.5$ vs 0.1. These exhibit the same level of selectivity, but are optimally effective for different ranges of Péclet number. APD is seen to provide comparable sensitivity to P, with one interesting advantage: the combination of longitudinal polarization and lateral diffusion allows the separation into different samples to be made on the *longitudinal* lengthscale L^* (Fig. 2) as opposed to the much smaller transverse dimension H^*. Thus, APD avoids the stringent geometric tolerances associated with stream splitting—particularly for multiple effluent fractions—in FFF (cf. Wahlund *et al.*, 1986) and SPLITT fractionation (cf. Giddings, 1985, 1986, 1988), where typical channel widths are fractions of 1 mm.

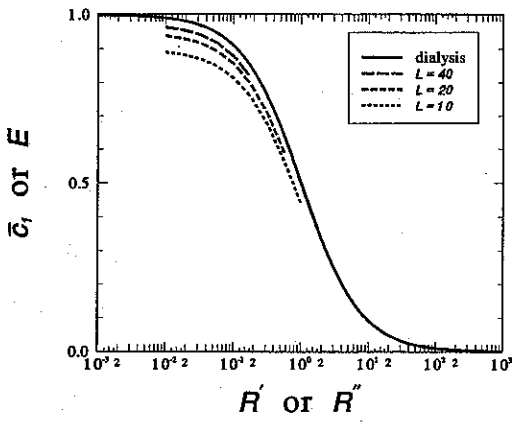

Fig. 11. Degree of antipolarization $\bar{c}_1$ as a function of reduced diffusional resistance R' at Péclet number $P = 1$, for three values of the aspect ratio: $L = 10$ vs 20 vs 40. Here the flow field corresponds to Fig. 6(a). For comparison, the fractional extraction curve $E(R'')$ representing conventional countercurrent dialysis is also shown.

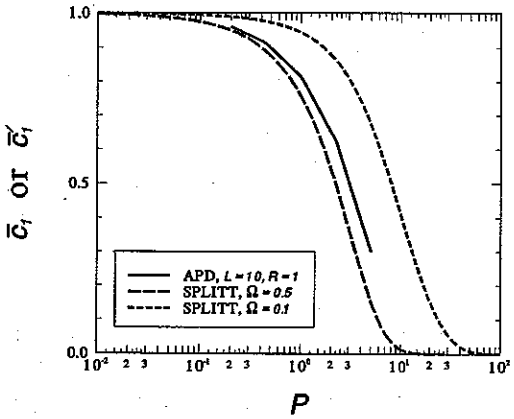

Fig. 12. Degree of antipolarization $\bar{c}_1$ as a function of Péclet number P at fixed membrane diffusional resistance $R = 1$. For comparison, analogous curves are shown for SPLITT fractionation, where (in contrast to APD) the splitting into two effluent fractions occurs in the *short* dimension of the cell.

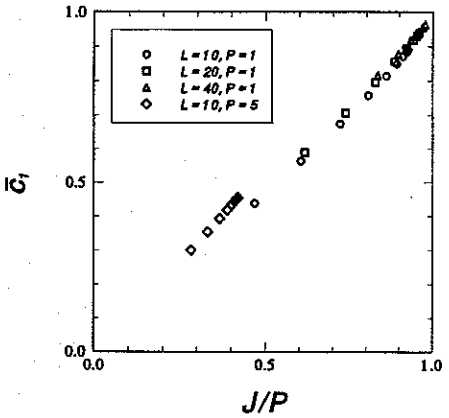

Fig. 13. Degree of antipolarization $\bar{c}_1$ correlated against reduced circulation flux J/P for four different sets of parameters.

The role of circulation flux in antipolarization

The aspect of counteracting convective polarization [Figs 8(a), 9(a), 10–12] has analogs in certain sedimentation–diffusion processes, where continuous rotation or intermittent flipping averages out the action of gravity in the reference frame of the container, and thereby leads to an "antisedimentation" effect (Dill and Brenner, 1983; Nadim *et al.*, 1985; Nitsche *et al.*, 1988). The case of steady rotation of a cylinder (former two references) leads to closed streamlines ("orbits") in the convective terms, which then implies the presence of a net circulation flux for the approximately uniform concentration distribution within the antisedimented zone.

In the present problem there is no rotation, but a direct connection can be established between the degree of antipolarization $\bar{c}_1$ and the circulation flux J. The concentration fields are nearly uniform throughout most of the flow channel, exhibiting more complex structure only at the ends. Thus, one can approximate the concentration throughout the cross section $x = L/2$ with $\bar{c}_1$, and neglect longitudinal diffusion. Thereby eq. (22) leads to the estimate

$$J/P \approx \bar{c}_1.$$

Figure 13 shows that this simplified picture represents the numerical results quite accurately. The good correlation between different aspect ratios L at $P = 1$ can be anticipated from Fig. 11; the comparison of $P = 1$ with $P = 5$ represents a more stringent confirmation.

CONCLUDING REMARKS

This paper has extended the idealized, plug-flow conception of antipolarization dialysis (Nitsche, 1994a) to analyze the impact of realistic considerations of construction upon the hydrodynamics, convection–diffusion and resultant selectivity with respect to membrane diffusional resistance R and Péclet number P of macrosolutes. Geometric and hydrodynamic details of implementing the desired flow field are shown not to have a strong influence upon the overall degree of antipolarization for $P \approx 1$, a regime in which APD compares favorably with conventional dialysis over the ranges of R and L investigated. Variations in R at fixed P would be approximated by a progression from globular (spherical) to elongated (rod-like) shape with the largest dimension remaining roughly constant. An increase in size for a fixed shape would increase both R and P, as was illustrated in Table 1 for spherical particles. The approach of APD is novel because of the manner in which it exploits two modes of selectivity *simultaneously*, as opposed to merely *magnifying* a particular physicochemical separation through interactions with another transport process.

Acknowledgements—The authors wish to thank Professors Charles Tier and Floyd B. Hanson, Department of Mathematics, Statistics, and Computer Science, University of Illinois at Chicago, for suggesting the eigenproblem reformulation of the discretized equations. Ms Michele L. Pertel and Mr Viral S. Lakhia assisted in surveying the literature. Financial support from the National Science Foundation (Grant No. CTS-9210277) is gratefully acknowledged.

Notes added in proof—A more recent, asymptotic investigation (Nitsche, L. C., 1995, A singular perturbation analysis of antipolarization dialysis at high aspect ratio, Preprint) shows that the leading-order selectivity curves of $\bar{c}_1$ vs R' at any fixed value of P (cf. Figs 10, 11) are equivalent—modulo a horizontal shift when R' is plotted on a logarithmic scale—to the fractional extraction formula (24) for conventional countercurrent dialysis. This conclusion removes the restriction of APD to $O(1)$ Péclet numbers, mentioned in connection with eq. (1), and would allow larger values of the flow velocity V^* and channel thickness H^* than those listed in Table 1. However, at larger P one must go to higher aspect ratio L to come close to the leading-order behavior. With reference to Fig. 10, the lower selectivity at $P = 5$ is thus explained: a sufficiently large aspect ratio (here numerically intractable) would bring the low-R' limit close to unity.

Given the eigenproblem reformulation of the discretized equations, the issue of conservative vs nonconservative finite-difference schemes is moot. Nonsingularity of the associated matrix (which precludes the telescopic concellation—i.e. numerical satisfaction of solute conservation—upon summing up the nodal equations) seems to be tied to the phenomenon of convective–diffusive polarization due to a solute-rejecting membrane: it occurs even in the simple one-dimensional example with constant coefficients (mentioned above in this connection). In any case, nodal equation is satisfied only to order $O(\lambda_{\min})$.

NOTATION

$A_{i,j}$	coefficients of singular basis functions for the flow field
c	concentration of solute
$\mathscr{C}_k$	set of coefficients $\{A_k, B_k, C_k, D_k\}$ for the kth flow-field singularity
C^n	regularity class of functions possessing n continuous derivatives
D	bulk diffusivity of solute
$\mathbf{e}_x, \mathbf{e}_y$	unit vectors in the x and y directions
F	stretching function for x coordinate grid distribution

G	stretching function for y coordinate grid distribution
$\mathscr{H}$	hindrance factor for pore diffusion of solute
H^*	width of the flow channel
J	number of poles for the flow-field singularities; also, circulation flux
$J_\parallel$	longitudinal flux of solute through the cross section $x = L/2$
$J_\perp$	lateral flux of solute across $y = 0$ for $L/2 < x < L$
K^*	hydraulic permeability coefficient of a membrane
ℓ^*	thickness of a membrane
L^*	length of the flow channel
L	dimensionless length of flow channel; aspect ratio, $L = L^*/H^*$
m	number of x coordinate grid intervals
M	modification factor for m due to nonuniform node distribution
n	number of y coordinate grid intervals
N	modification factor for n due to nonuniform node distribution
p	pressure in the fluid
P	pressure field of angular singularity in velocity; also, solute Péclet number based width H^* and velocity V^*
$P^{[i]}$	singular basis function for pressure
$\mathbf{r}$	position vector
$\hat{\mathbf{r}}$	position vector of the pole of a singular solution
R	distance from a pole $\hat{\mathbf{r}}$, $R = \sqrt{X^2 + Y^2}$; also, dimensionless diffusional resistance to solute of a membrane
R'	reduced membrane diffusional resistance, $R' = R/L$
R''	reduced membrane resistance pertaining to conventional dialysis
$\mathbf{R}$	position vector relative to the pole $\hat{\mathbf{r}}$, $\mathbf{R} = \mathbf{r} - \hat{\mathbf{r}}$
$\mathbf{u}$; u_x, u_y	regularized fluid velocity vector; its x and y components
$\mathbf{U}^{[i]}$; $U_x^{[i]}, U_y^{[i]}$	singular basis function for $\mathbf{u}(\mathbf{r})$; its x and y components
$\mathbf{v}$; v_x, v_y	fluid velocity vector; its x and y components
$v_\perp$	normal velocity at a porous surface
V^*	mean flow velocity through channel
$\mathbf{V}$; V_x, V_y	velocity vector for angular discontinuity; its x and y components
x, y	Cartesian position coordinates
$\hat{x}, \hat{y}$	Cartesian coordinates of the pole of a singular solution
X, Y	Cartesian position coordinates relative to the pole $(\hat{x}, \hat{y})$, $X = x - \hat{x}$, $Y = y - \hat{y}$

Greek letters

α	terminal grid expansion factor between the ends of the flow channel
β	terminal grid compression factor for the singularities in the flow field
γ	areal porosity of a membrane
η	auxiliary variable for generating nonuniform y coordinate grid
ξ	auxiliary variable for generating nonuniform x coordinate grid
ϕ	regularized stream function
ψ	stream function
Ψ	stream function for angular discontinuity in velocity
Ω	fractional distance between splitter plate and "accumulation wall" in SPLITT fractionation [see e.g. Giddings (1986)].

Superscripts

[1]	point source
[2]	point force in the x direction
[3]	point force in the y direction
[i]	ith type of singular velocity basis function
(B)	base flow field consisting of two angular singularities and the fully developed parabolic velocity profile
*	indicates dimensional variable

Subscripts

i	index of x grid points; type of singular velocity basis function
j	index of y grid points; index of poles for singular velocity basis functions
k	index of flow-field singularity

Marks over symbols

^	pertains to the pole of a singular velocity basis function
~	indicates inner asymptotic flow field depending on scaled position vector

REFERENCES

Bird, R. B., Stewart, W. E. and Lightfoot, E. N., 1960, *Transport Phenomena*. Wiley, New York.

Bohrer, M. P., Patterson, G. D. and Carroll, P. J., 1984, Hindered diffusion of dextran and ficoll in microporous membranes. *Macromolecules* **17**, 1170–1173.

Bruns, F. W., 1979, Numerical calculation on creeping flow in a closed cylindrical cavity. *Comp. Fluids* **7**, 257–265.

Bruns, F. W., 1980, A moving solid–fluid–solid contact line: the removal of the force and pressure singularity by a slip and filtration flow. *J. Colloid Interface Sci.* **74**, 341–348.

Colton, C. K., Smith, K. A., Stroeve, P. and Merrill, E. W., 1971, Laminar flow mass transfer in a flat duct with permeable walls. *A.I.Ch.E. J.* **17**, 773–780.

Costar Corporation, 1992, *Life Science Filtration Catalog*. Cambridge, MA.

Dąbroś, T., 1985, A singularity method for calculating hydrodynamic forces and particle velocities in low-Reynolds-number flows. *J. Fluid Mech.* **156**, 1–21.

Dahlquist, G. and Björck, Å., 1974, *Numerical Methods* (Transl. by N. Anderson). Prentice-Hall, Englewood Cliffs, NJ.

Deen, W. M., 1987, Hindered transport of large molecules in liquid-filled pores. *A.I.Ch.E. J.* **33**, 1409–1425.

Dill, L. H. and Brenner, H., 1983, Taylor dispersion in systems of sedimenting nonspherical Brownian particles. III. Time-periodic forces. *J. Colloid Interface Sci.* **94**, 430–450.

Dongarra, J. J., Bunch, J. R., Moler, C. B. and Stewart, G. W., 1979, *LINPACK Users' Guide*. Society for Industrial and Applied Mathematics (SIAM), Philadelphia.

Giddings, J. C., 1985, A system based on split-flow lateral-transport thin (SPLITT) separation cells for rapid and continuous particle fractionation. *Sep. Sci. Technol.* **20**, 749–768.

Giddings, J. C., 1986, Crossflow gradients in thin channels for separation by hyperlayer FFF, SPLITT cells, elutriation, and related methods. *Sep. Sci. Technol.* **21**, 831–843.

Giddings, J. C., 1988, Continuous separation in split-flow thin (SPLITT) cells: potential applications to biological materials. *Sep. Sci. Technol.* **23**, 931–943.

Giddings, J. C., 1993, Field-flow fractionation: analysis of macromolecular, colloidal, and particulate materials. *Science* **260**, 1456–1465.

Giddings, J. C., Yang, F. J. and Myers, M. N., 1976a, Theoretical and experimental characterization of flow field-flow fractionation. *Anal. Chem.* **48**, 1126–1132.

Giddings, J. C., Yang, F. J. F. and Myers, M. N., 1976b, Flow field-flow fractionation: a versatile new separation method. *Science* **193**, 1244–1245.

Giddings, J. C., Yang, F. J. and Myers, M. N., 1977a, Flow field-flow fractionation: new method for separating, purifying, and characterizing the diffusivity of viruses. *J. Virology* **21**, 131–138.

Giddings, J. C., Yang, F. J. and Myers, M. N., 1977b, Flow field-flow fractionation as a methodology for protein separation and characterization. *Anal. Biochem.* **81**, 395–407.

Giddings, J. C., Yang, F. J. and Myers, M. N., 1977c, The flow field-flow fractionation channel as a versatile pressure dialysis and ultrafiltration cell. *Sep. Sci.* **12**, 499–510.

Gupta, M. M., Manohar. R. P. and Noble, B., 1981, Nature of viscous flows near sharp corners. *Comp. Fluids* **9**, 379–388.

Hancock, C., Lewis, E. and Moffatt, H. K., 1981, Effects of inertia in forced corner flows. *J. Fluid Mech.* **112**, 315–327.

Harper, J. F. and Wake, G. C., 1983, Stokes flow between parallel plates due to a transversely moving end wall. *IMA J. Appl. Math.* **30**, 141–149.

Hermans, J. J., 1979, Some aspects of counter current dialysis through hollow fiber membranes. *Recueil, J. Roy. Netherlands Chem. Soc.* **98**, 133–136.

Ingham, D. B. and Kelmanson, M. A., 1984, *Boundary Integral Equation Analyses of Singular, Potential, and Biharmonic Problems*, Lecture Notes in Engineering, Vol. 7. Springer, New York.

Jennings, A. and McKeown, J. J., 1992, *Matrix Computation*, 2nd Edition. Wiley, New York.

King, S. P., 1988, Aspects of diffusion in microporous membranes. *Chemica Scripta* **28**, 161–172.

Klein, E., Ward, R. A. and Lacey, R. E., 1987, Membrane processes—dialysis and electrodialysis, in *Handbook of Separation Process Technology* (Edited by R. W. Rousseau), Chap. 21. Wiley-Interscience, New York.

Lee, H. L. and Lightfoot, E. N., 1976, Preliminary report on ultrafiltration-induced polarization chromatography—an analog of field-flow fractionation. *Sep. Sci.* **11**, 417–440.

Moffatt, H. K., 1964, Viscous and resistive eddies near a sharp corner. *J. Fluid Mech.* **18**, 1–18.

Nadim, A., Cox, R. G. and Brenner, H., 1985, Transport of sedimenting Brownian particles in a rotating Poiseuille flow. *Phys. Fluids* **28**, 3457–3466.

Nitsche, L. C., 1994a, Pseudo-sedimentation dialysis: an elliptic transmission problem. *Quart. Appl. Math.* **LII**, 83–102.

Nitsche, L. C., 1994b, One-dimensional stretching functions for C^n patched grids, and associated truncation errors in finite-difference calculations. Preprint.

Nitsche, L. C. and Brenner, H., 1990, Hydrodynamics of particulate motion in sinusoidal pores via a singularity method. *A.I.Ch.E. J.* **36**, 1403–1419.

Nitsche, L. C., Nitsche, J. M. and Brenner, H., 1988, Existence, uniqueness and regularity of a time-periodic probability density distribution arising in a sedimentation–diffusion problem. *SIAM J. Math. Anal.* **19**, 153–166.

Noda, I., Brown-West, D. G. and Gryte, C. C., 1979, Effect of flow maldistribution on hollow fiber dialysis—experimental studies. *J. Membrane Sci.* **5**, 209–225.

Noda, I. and Gryte, C. C., 1981, Multistage membrane separation processes for the continuous fractionation of solutes having similar permeabilities. *A.I.Ch.E. J.* **27**, 904–912.

Pan, F. and Acrivos, A., 1967, Steady flows in rectangular cavities. *J. Fluid Mech.* **28**, 643–655.

Park, J. K. and Chang, H. N., 1986, Flow distribution in the fiber lumen side of a hollow-fiber module. *A.I.Ch.E. J.* **32**, 1937–1947.

Pozrikidis, C., 1992, *Boundary Integral and Singularity Methods for Linearized Viscous Flow*. Cambridge University Press, New York.

Ray, R., Wytcherley, R. W., Newbold, D., McCray, S., Friesen, D. and Brose, D., 1991, Synergistic, membrane-based hybrid separation systems. *J. Membrane Sci.* **62**, 347–369.

Shaw, R. A., Deluca, R. and Gill, W. N., 1972, Reverse osmosis: increased productivity by reduction of concentration polarization in laminar flow reverse osmosis using intermediate non-rejecting membrane sections. *Desalination* **11**, 189–205.

Taylor, G. I., 1958, On scraping viscous fluid from a plane surface, in *The Scientific Papers of Sir Geoffrey Ingram Taylor*, Vol. IV (Edited by G. K. Batchelor), pp. 410–413. Cambridge University Press, Cambridge.

Taylor, G. I., 1960, Similarity solutions of hydrodynamic problems, in *Aeronautics and Astronautics* (Durand Centen. Conf. Vol.) (Edited by N. J. Hoff and W. G. Vincenti), pp. 21–28. Pergamon Press, Oxford.

Thompson, J. F. and Mastin, C. W., 1985, Order of difference expressions in curvilinear coordinate systems. *J. Fluids Engng* **107**, 241–250.

Thompson, J. F., Warsi, Z. U. A. and Mastin, C. W., 1985, *Numerical Grid Generation. Foundations and Applications*. North-Holland, New York.

Wahlund, K.-G., Winegarner, H. S., Caldwell, K. D. and Giddings, J. C., 1986, Improved flow field-flow fractionation system applied to water-soluble polymers: programming, outlet stream splitting, and flow optimization. *Anal. Chem.* **58**, 573–578.